International Journal of the Korean Society of Precision Engineering Vol. 1, No. 1, June 2000.

Hardening of Steel Sheets with Orthotropy Axes Rotations and Kinematic Hardening

Ju-Hee Hahm*, Kwon-Hee Kim**, and Jung-Je Yin***

*Department of Mechanical Engineering, Korea University, Seoul, South Korea, **Department of Mechanical Engineering, Korea University, Seoul, South Korea and ***Department of Mechanical Engineering & Design, Induk Institute of Technology, Seoul, South Korea

ABSTRACT

Anisotropic work hardening of cold rolled low carbon steel sheets is studied. The experiments consist of two stage tensile prestraining and tensile tests. At the first prestraining, steel sheets are stretched along the rolling direction by 3% and 6% tensile strains. The second prestrains are at 0° , 30° , 60° , 90° to the rolling directions by varying degrees. Tensile tests are performed on the specimens cut from the sheets after the two stage prestraining. A theoretical framework on anisotropic hardening is proposed which includes Hill's quadratic yield function, Ziegler's kinematic hardening rule, and Kim and Yin's assumption on the rotation of orthotropy axes. The predicted variations of R-values with second stage tensile strain are compared with the experimental data.

Key Words : sheet, anisotropic hardening, isotropic hardening, kinematic hardening, orthotropy axes, rotation, plastic work, R-value, quadratic yield function, back stress

1. Introduction

Theory of anisotropy for sheet metals are very important for the industrial applications. Generally, it consists of yield function and hardening rule. Among the yield functions, Hill's quadratic yield function [1] is simple and widely used in applications. It is satisfactory for the sheet metals with R>1, where R is plastic strain ratio (or R-value). In the case of R<1, such as in aluminum, "anomalous behavior" has been observed [2,3]. Numerous non-quadratic yield function has been proposed in the literature to account for the anomaly [4-6]. But they are generally quite complex and are not widely applied in. Recent study by Han *et al.* [7]

Another important issue in applying the anisotropy theory is the rotation of orthotropy axes when the principal directions of strains are not coincident with the orthotropy axes [8-12]. The rotation of orthotropyaxes should be a part of the constitutive theory of orthotropic anisotropy.

In this study a theoretical framework on anisotropic hardening is proposed, which includes Hill's quadratic yield function, Ziegler's kinematic hardening rule [13], and Kim and Yin's assumption [9] on the rotation of orthotropy axes. With the proposed constitutive model, variations of R-values are predicted and compared with the experimental data for prestrained anisotropic states.

2. Experiments

Cold rolled sheets of a low carbon steel(AK steel, model SPC3) have been selected for experiments. Cold rolled sheets of a low carbon steel(AK steel, model SPC3) have been selected for experiments. Tensile prestrains of 3% and 6% are applied to the full size sheets along the rolling direction. After the prestrains, second prestrains of 1%, 2%, 5%, 10% and 15% are applied at 30°, 45°, 60° and 90° to the rolling direction. Table 1 shows the combinations of

the prestrains which are used in the experiment. Depending upon the orientation of the second prestrain axis tensile necking is observed during prestraining. After the second prestrains, tensile tests have been performed at every 10° from the tensile axis of the second prestrains(see Fig1). From the tensile tests, stress - strain relations and R-values have been measured. From the distributions of yield stress for the combinations of prestrains, rotation of orthotropy axes has been verified. Fig. 2 shows various angles defined for the description of orientation change of orthotropy axes. Further details of the experiments can be found in Yin [10].

During the tensile tests strains have been measured in the longitudinal and transverse directions. Thickness plastic strain can be calculated from the plastic strains in the longitudinal and transverse directions from the condition of volume contancy. Fig. 3 shows a typical pattern of transverse plastic strain ε_w^p and thickness plastic strain ε_t^p plotted against longitudinal plastic strain ε_l^p.

Rotations of the orthotropy axes will affect the incremental R-value if flow normality continue to exist. From the measured strains incremental R-value can be obtained as $R = |d\varepsilon_w^p / d\varepsilon_t^p|$. Fig. 4 shows variations of the incremental R-value at angles to the rolling direction.

Table 1. Combinations of first and second tensile prestrains

1st prestrain	Angle(ψ)	2nd prestrain(%)				
3 %	30°	1	2	5	10	-
	45°	1	2	5	10	-
	60°	1	2	5	10	-
	90°	-	2	5	10	15
6 %	30°	1	2	5	10	-
	45°	1	2	necking	necking	-
	60°	1	necking	necking	necking	-
	90°	-	2	5	10	15

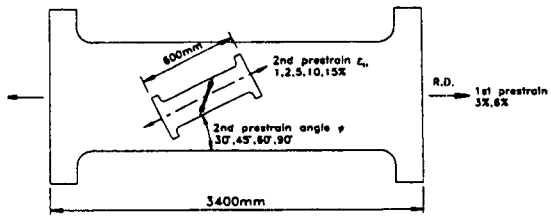

Fig. 1 Schematic illustration of the experimental procedures

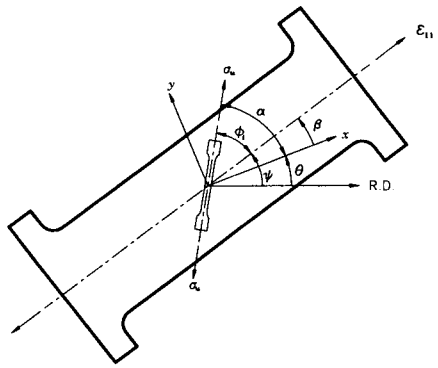

Fig. 2 Definition of various angles. ψ : 2nd prestrain (ε_{11}) axis angle from the rolling direction, θ : x-axis angle from the rolling direction, β : 2nd prestrain axis angle from the x-axis, α :tensile angle from the x-axis, ϕ_t : tensile angle from 2nd prestrain axis, σ_u : uniaxial tensile stress

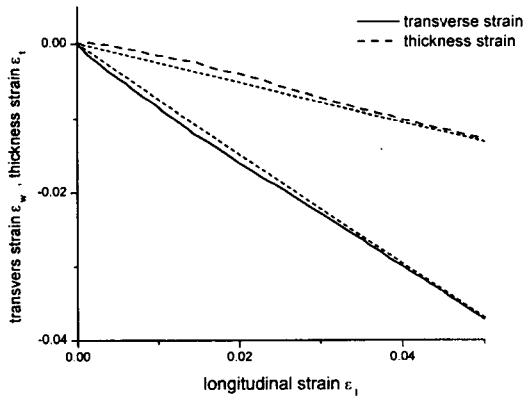

Fig. 3 A typical pattern of measured longitudinal strain ε_l^p and transverse strain ε_w^p and thickness strain ε_t^p

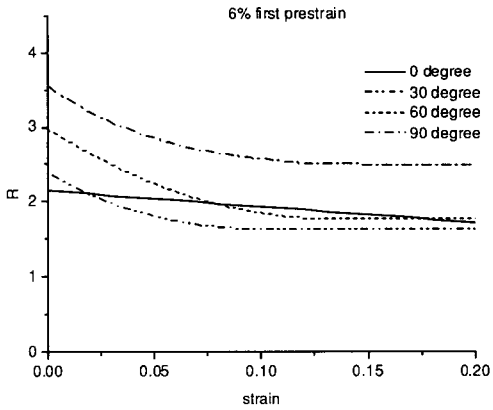

Fig. 4 Variations of incremental R-value during the second tensile prestraining after the first prestrain of 6% in the rolling direction

3. Anisotropic hardening with rotation of orthotropy axes

3.1 Rotation of orthotropy axes

Kim and Yin[9] suggested that the rate of orientation change of the orthotropy axes during the second prestraining is proportional to the shear strain rate with respect to the principal directions of stress. In term of the angle β shown in Fig. 2, this can be stated as

$$d\beta = (1+C)d\varepsilon_{12} \qquad (1)$$

where 1 and 2 represent the tensile loading direction and the transverse direction for the second prestraining and C is a constant which is dependent upon the state of hardening. In (1) it is assumed that the simple shear is induced by shear strain $d\varepsilon_{12}$ within the gauge section of the tensile specimen. Thus the rotation of the orthotropy axes can be decomposed into rigid rotation by simple shear and strain induced rotation represented by $d\varepsilon_{12}$ and $Cd\varepsilon_{12}$, respectively. In actual tests, however, it is difficult to achieve simple shear in the gauge section completely free from the end constraints due to the specimen geometry. Grips have been designed to minimize constraint against simple shear for the second prestraining.

3.2 Isotropic hardening coupled with kinematic hardening

For the sake of simplicity, we assume that the yield surface shape remains similar in the $\sigma_x - \sigma_y - \tau_{xy}$ stress space and the volume of yield surface is monotonically increasing function of plastic work. Here, x and y represent orthotropy axes which are along the rolling and transverse directions initially. With Hill's quadratic yield function, the yield surface becomes an ellipsoid. With kinematic hardening, the yield surface will migrate in the $\sigma_x - \sigma_y - \tau_{xy}$ stress space. According to Ziegler, the center of the yield surface moves continuously in the $(\sigma - \alpha)$ direction during plastic deformation where σ and α represent the current state of stress and the center of the yield surface, respectively. The yield condition of isotropic hardening coupled with kinematic hardening for plane stress becomes

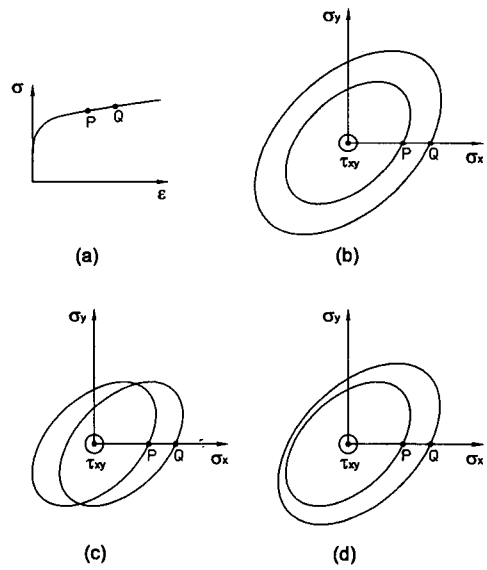

Fig. 5 Schematic descriptions of isotropic hardening coupled with kinematic hardening in the $\sigma_x - \sigma_y - \tau_{xy}$ stress space.

(a) uniaxial stress-strain curve
(b) isotropic hardening in plane stress
(c) kinematic hardening in plane stress
(d) isotropic hardening coupled with kinematic hardening in plane stress

$$(G+H)(\sigma_x-\alpha_x)^2-2H(\sigma_x-\alpha_x)(\sigma_y-\alpha_y) + (H+F)(\sigma_y-\alpha_y)^2+ 2N(\tau_{xy}-\alpha_{xy})^2=1 \quad (2)$$

or, upon rewriting

$$(g+h)(\sigma_x-\alpha_x)^2-2h(\sigma_x-\alpha_x)(\sigma_y-\alpha_y) + (h+f)(\sigma_y-\alpha_y)^2+2(\tau_{xy}-\alpha_{xy})^2=\frac{1}{N} \quad (3)$$

Here $f=F/N$, $g=G/N$, $h=H/N$ are constants for fixed yield surface shape and the value of N is dependent upon isotropic hardening. The center of the yield surface changes during plastic deformation such as

$$d\boldsymbol{\alpha} = q(\boldsymbol{\sigma}-\boldsymbol{\alpha})d\mu, 0 \le q \le 1 \quad (4)$$

where

$$d\mu = \frac{d\boldsymbol{\sigma}\cdot d\boldsymbol{\varepsilon}^p}{(\boldsymbol{\sigma}-\boldsymbol{\alpha})\cdot d\boldsymbol{\varepsilon}^p} \quad (5)$$

Here, the factor q represents the degree of kinematic hardening. When $q=1$ with constant value of N, the equation (4) represents Ziegler's pure kinematic hardening rule. When $q=0$, the equation (4) represents pure isotropic hardening. The case of $0<q<1$ corresponds to isotropic hardening coupled with kinematic hardening. Fig. 5 illustrates three cases of pure isotropic hardening, pure kinematic hardening and isotropic hardening coupled with kinematic hardening. The plastic work can be decomposed as

$$dW^p = \boldsymbol{\sigma}\cdot d\boldsymbol{\varepsilon}^p=(\boldsymbol{\sigma}-\boldsymbol{\alpha})\cdot d\boldsymbol{\varepsilon}^p + \boldsymbol{\alpha}\cdot d\boldsymbol{\varepsilon}^p = dW_i^p + dW_k^p \quad (6)$$

with

$$dW_i^p = (\boldsymbol{\sigma}-\boldsymbol{\alpha})\cdot d\boldsymbol{\varepsilon}^p,$$
$$dW_k^p = \boldsymbol{\alpha}\cdot d\boldsymbol{\varepsilon}^p \quad (7)$$

From equation (6) and (7), equation (5) can be rewritten as

$$d\mu = \frac{d\boldsymbol{\sigma}\cdot d\boldsymbol{\varepsilon}^p}{(\boldsymbol{\sigma}-\boldsymbol{\alpha})\cdot d\boldsymbol{\varepsilon}^p} = \frac{d\boldsymbol{\sigma}\cdot d\boldsymbol{\varepsilon}^p}{dW^p-dW_k^p} = \frac{d\boldsymbol{\sigma}\cdot d\boldsymbol{\varepsilon}^p}{dW_i^p} \quad (8)$$

Here dW_i^p and dW_k^p are portions of plastic work corresponding to isotropic hardening and kinematic hardening respectively. We assume that the yield surface volume is a function of isotropic portion of plastic work $W_i^p = \int dW_i^p$. With constant values of f, g and h, this assumption leads to

$$N = N(W_i^p) = N(\int dW_i^p) \quad (9)$$

The quantitative evaluation of the orthotropy axes rotation, kinematic hardening and isotropic hardening represented by equations (1) - (9) can be made from the tensile test data for the combinations of prestrains summarized in Table 1. The values of C, f, g, h and q are determined such that they fit the data best. The general agreement between the experiment and prediction is good for the rotations of orthotropy axes. The details of the rotations of orthotropy axes can be found in Yin [10] and Kim and Yin [9]. The value of q can be determined from the plane stress yield locus after the 6% first prestrain. It is assumed that the value of q remains constant. In this work, the focuse will be given to the flow behavior of the prestrained sheets.

4. Predicted R-values

4.1 Isotropic hardening with rotation of the orthotropy axes

Fig. 3 shows a typical patterns of transverse strain ε_w^p and thickness strain ε_t^p plotted against longitudinal strain ε_l^p after the first prestrain. At the beginning of the longitudinal strain ($0<\varepsilon_l^p<0.04$), the transverse strain decreases rapidly before it converges to a steady rate of decrease afterwards ($\varepsilon_l^p>0.04$). Due to this transient behavior, R-value

decreases rapidly within the range ($0<\varepsilon_1^p<0.04$) and reaches a steady state value later as shown in Fig. 4. The rapid decrease of R-value at the lower strain range becomes prominent with the increasing loading angle ϕ. It is interesting to note that when $\phi=0^\circ$ measured R-value continues to decrease for the entire strain range. According to isotropic hardening with the rotations of orthotropy axes R-values are expected to stay at constant values at $\phi=0^\circ$ and $\phi=90^\circ$ since there are no rotations of orthotropy axes.

At $\phi=30^\circ$ and $\phi=60^\circ$, the predicted R-value increases initially due to rotations of the orthotropy axes and converges to a constant value. Predicted R-values at different loading directions of $\phi=0^\circ$, 30° , 60° and 90° are shown in Fig. 6 against the experimental data. There are clear discrepancies between the experimental data and the predictions.

4.2 Isotropic hardening coupled with kinematic hardening

With the discrepancies mentioned above, it seem logical to introduce the possibility of kinematic hardening. With the introduction of kinematic hardening R-value will be determined by the interplay between the yield surface migration in the stress space and the rotations of the orthotropy axes. To determine the degree of kinematic hardening represented

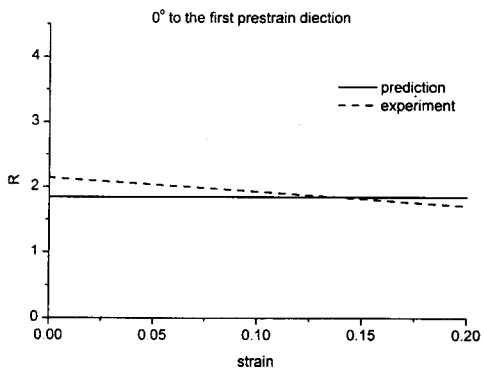

(a)

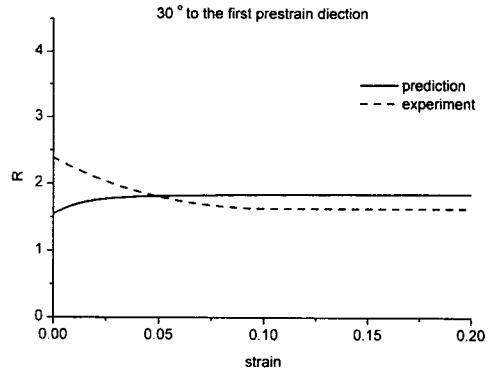

(b)

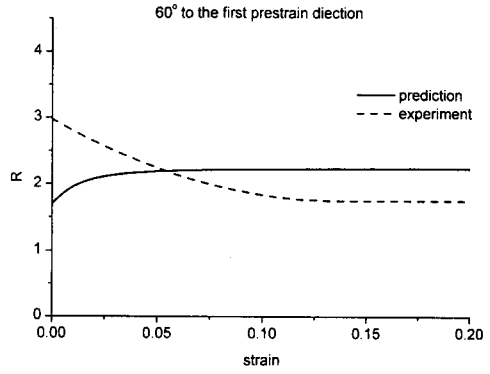

(c)

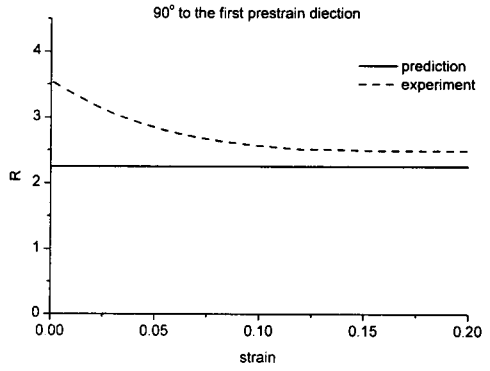

(d)

Fig. 6 R-values predicted based upon isotropic hardening and rotation of orthotropic axes for the first prestrain of 6% in the rolling direction
(a) 0 ° to the first prestrain direction
(b) 30 ° to the first prestrain direction
(c) 60 ° to the first prestrain direction
(d) 90 ° to the first prestrain direction

by the value of q in equation (4), the centers of yield surface for the first prestrain of 0%, 3% and 6% have been calculated based upon equation (4) and (5) with least square fit to the yield stress data. After the first prestrains, yield surface center will be on the x axis in the $\sigma_x - \sigma_y - \tau_{xy}$ stress space. With this assumption, it is possible to calculate the magintude α_x of the back stress $\boldsymbol{\alpha} = (\alpha_x, 0, 0)$ in the $\sigma_x - \sigma_y - \tau_{xy}$ stress space and hence the portions of isotropic and kinematic hardening in the plastic work. The calculated portion of isotropic hardening work is 85% of total plastic work and that of kinematic hardening work is 15%. From the calculated portions of plastic work, the factor q and the initial back stress α_x are determined as 0.15 and 3 kgf/mm^2, respectively after the first prestrain of 6%. Fictitious case of $q = 0.4$ and initial back stress α_x = 3.5 kgf/mm^2 is presented in Fig. 7 for comparison. With the introduction of kinematic hardening, predicted R-values decrease slightly with the tensile longitudinal strain. This seems to be an improvement over the predicted values in Fig. 6. However, the predicted R-values even with kinematic hardening do not show good agreements with the experimental data.

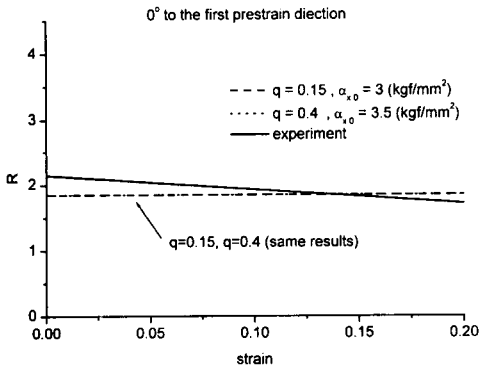

(a)

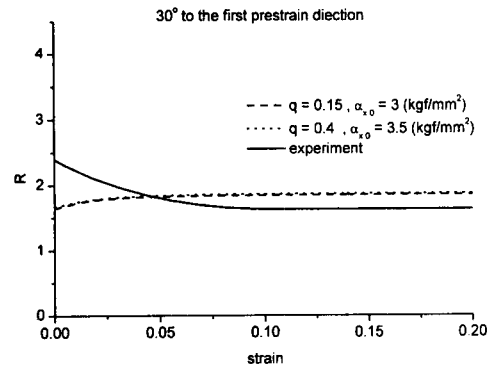

(b)

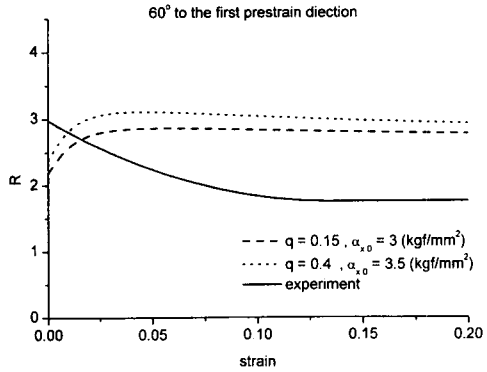

(c)

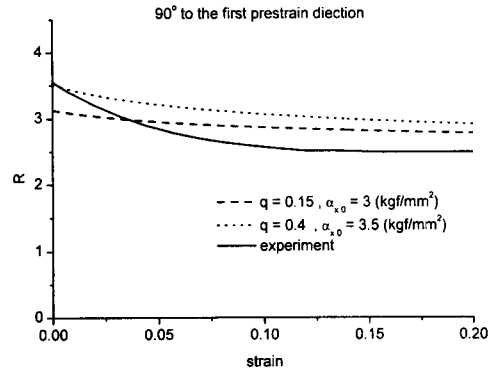

(d)

Fig. 7 R-values predicted based upon isotropic hardening coupled with kinematic hardening and rotation of orthotropic axes for the first prestrain of 6% in the rolling direction
(a) 0 ° to the first prestrain direction
(b) 30 ° to the first prestrain direction
(c) 60 ° to the first prestrain direction
(d) 90 ° to the first prestrain direction

5. Conclusion

Anisotropic hardening of steel sheets has complex nature. Rotation of orthotropy axes is observed when the tensile loading direction is not coincident with one of the orthotropy axes. Measured tensile stress-strain relation is dependent upon the loading direction with respect to the orthotropy axes. R-value is dependent upon the strain and the orientation of the tensile axis. There seems to be no appropriate theory which can deal with such complex behavior.

In an attempt to develop a theoretical framework of anisotropic hardening, Hill's quadratic yield function, Ziegler's kinematic hardening rule, and Kim and Yin's assumption on the rotation of orthotropy axes have been integrated for the prediction of R-value. Considering isotropic hardening with rotation of orthotropy axes, monotonic increase in the R-value is predicted during tensile loading. When kinematic hardening is incorporated, mild decrease in the R-value is predicted at 60° and 90° after 6% first prestrain. It is apparent that current theoretical framework does not predict initial radical decrease in R-value experimentally observed. Further study seems to be necessary to understand the phenomenon and to establish a theoretical framework which can represent microstructural evolutions such as texture reorganization and back stress development.

References

1. Hill, R., 1948, "A theory of yielding and plastic flow of anisotropic metals," Proceedings of Royal Society of London, A193, p. 281.
2. Pearce, R., 1968, "Some aspects of anisotropic plasticity in sheet metals," Int. J. Mech. Sci., Vol. 10, p. 995.
3. Woodthorpe, J. and Pearce, R., 1970, "The anomalous behavior of aluminum sheet under balanced biaxial tension," Int. J. Mech. Sci., Vol. 12, p. 341.
4. Hill, R., 1979, "Theoretical plasticity of textured aggregates," Math. Proc. Camb. Phil. Soc., Vol. 85, p. 179.
5. Hill, R., 1990, "Constitutive modelling of orthotropic plasticity in sheet metals," J. Mech. Phys. Solids, Vol. 38, p. 405.
6. Bassani, J. L., 1977, "Yield characterization of metals with transversely isotropic plastic properties," Int. J. Mech. Sci., Vol. 19, p. 651.
7. Han-Chin Wu, Hong-Ki Hong and Ya-Po Shiao, 1999, "Anisotropic plasticity with application to sheet metals," Int. J. Mech. Sci. Vol. 41, p. 703.
8. Kim, K. H., 1992, "Evolution of anisotropy during twisting of cold drawn tubes," J. Mech. Phys. Solids, Vol. 40, p. 127.
9. Kim, K. H. and Yin, J. J., 1997, "Evolution of anisotropy under plane stress," J. Mech. Phys. Solids, Vol. 45, No. 5, p. 841.
10. Yin, J. J., 1992, "A study on the strain hardening characteristics of anisotropic sheet metals," Ph.D. Thesis, Seoul National University, Korea
11. Arrieux, R., Vacher, P. and Nguyen, T., 1996, "A Method to Predict the Onset of Necking in Numerical Simulation of Deep Drawing Operations," Annals of the CIRP, Vol. 45/1, p.255.
12. Nguyen Nhat, T., Arrieux, R., Vacher, P. and Tabourot, L., 1998, "Plasticity Instability for off-axes Loading in Deep-drawing operation," J. Mat. Processing Technology 77., p. 175.
13. Ziegler, H., 1959, "A modification of Prager's hardening rule," Q. Appl. Math. 17, p.55.